Simulating effective potential under strain for holes

A. Mendoza-Álvarez[a], L. Diago-Cisneros[a,b], J.J. Flores-Godoy[c] and G. Fernández-Anaya[a]
[a]*Departamento de Física y Matemáticas, Universidad Iberoamericana, CDMX, 01219, México.*
e-mail: ldiago@fisica.uh.cu
[b] *Facultad de Física, Universidad de La Habana, 10400, Cuba.*
[c]*Departamento de Matemática, Facultad de Ingeniería y Tecnologías*
Universidad Católica del Uruguay Montevideo, Uruguay.

Received 29 July 2015; accepted 9 May 2016

The effective potential ($V_{\rm eff}$) evolution, is graphically illustrated for an increasing mixing of heavy- and light-holes (*lh*) under strain. The impact of the present study is enlarged provided we were able to deduce comprehensive analytic expressions for the valence-band offset both for zinc blende and wurtzite semiconductors, useful in current solid-state physics studies, whenever one manages to manipulate the accumulated pseudomorphic strain and mixing effects in a single shoot. We found permutations of $V_{\rm eff}$ character for *lh*, that retrieve the hypothetically predicted striking "*keyboard*" effect. Interestingly, the strain diminishes the *keyboard* profile, and also makes it emerge or vanish occasionally. Due in-plane anisotropy the *keyboard* effect under pseudomorphic stress turns topologically tuned. We conclude that multiband-mixing and stress-induced events, are strong competitor mechanisms that can not be universally neglected by assuming a fixed-height $V_{\rm eff}$, as a reliable none-mutable test-run input for layered systems. Our results may be of relevance for promising tunable heterostructure's design to enhance the hole mobility in semiconductor devices.

Descriptores: Effective scattering potential; valence-band mixing; pseudomorphic strain; valence-band offset.

PACS: 71.70.Ej; 72.25.Dc; 73.21.Hb; 73.23.Ad

1. Synopsis of Fundamentals and Motivation

For many actual practical solutions and technological applications, due to the impressive development of low-dimensional electronic and optoelectronic devices, it is drastically important to include the valence-band mixing [1], *i.e.* the degree of freedom transverse to the main transport direction, whenever the holes are involved. Previous theoretical studies had focused this topic in resonant tunneling [2] and had pointed up its relevance for experimental and technological applications [1]. If the electronic transport through these systems, engage both electrons and holes, the low-dimensional device response *threshold* depends on the slower-heavier charge-carrier's motion through specific potential regions [3]. It is unavoidable to recognize that in the specialized literature there is plenty of reports studying several physical phenomena derived from hole mixing effects and strain, *via* standard existing methods. Some authors had managed to determine optimal situations in a resonant tunneling of holes under internal strains, disregarding scattering effects and assuming a spatial symmetry for a constant potential [4]. A first-principles study on valence-band (VB)-mixing, established a non-linear response for a pseudo-potential in series of the atomic distribution function [5]. Over the past few decades VB-mixing and/or strain had been extensively studied in several nanostructures ranging from quantum wells [4, 6–8] to quantum wires [9, 10] and to quantum dots [11]. However, just a few reports are available regarding the very evolution itself of the effective potential due to several causes, as a central topic of research. We do not focus in the present paper on the VB-mixing and strain effects problem themselves, but rather on the evolution of the effective potential when tuning both effects and on their possible influence over the scattering properties. We hope to make some progress in the understanding of the underlying physics as well as determining whether or not the VB-mixing and strain are competitor mechanisms in the evolution of the effective potential. Few direct measurements –if any– are available because they have not been usually carried out on the subject. We hope to trigger further experimental works on hole-coupling effects and strain phenomenon in the same setup, even in complementary fields whenever scattering events of mixed holes through stressed heterostructures are involved.

Earliest striking elucidations due to Milanović and Tjapkin for electrons, [12] and recalled much later by Pérez-Álvarez and García-Moliner for a fully unspecific multiband theoretical case [14], are fundamental cornerstones in this concern. The metamorphosis of the effective *band offset* potential $V_{\rm eff}$, "felt" by charge carriers depending on the transverse momentum value, is a very persuasive workbench to graphically mimic, the phenomenon of the in-plane dependence of the effective mass, widely known as the VB-mixing for holes. In a few words, a hole band mixing is crucial for bulk and low-dimensional confined systems possessing quantal heterogeneity, as shall be discussed in this paper, similarly to the single-band-electron problem [12] and somehow to the unstrained multiband-hole problem [13]. Particularities of the appealing evolution features of $V_{\rm eff}$ for holes, in the presence of gradually increasing VB-mixing under strain and assuming their effects are well understood, could be of interest for condensed-matter physicists, working in the area of quantum transport through standard quantum barrier(QB)–quantum well(QW) layered systems in multiband-multichannel models.

As common assertion, the $V_{\rm eff}$ input value derives from bulk *band offset* lineup as long as the transverse momentum ($\kappa_{\rm T}$) values are negligible [14]. For finite $\kappa_{\rm T}$, this assertion

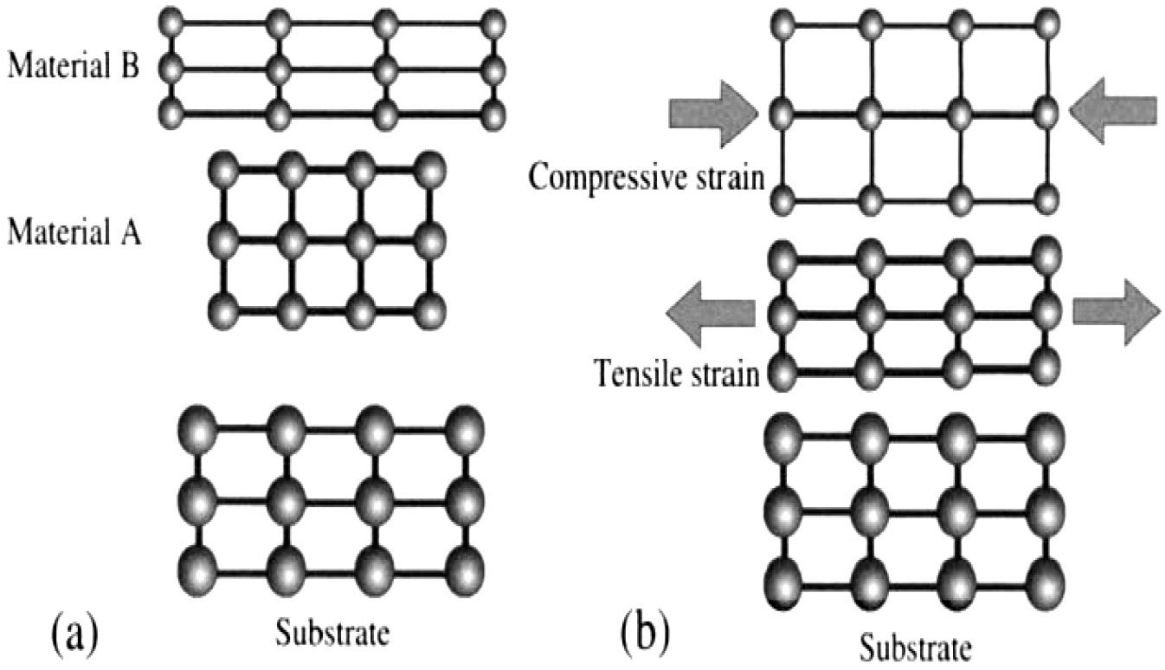

FIGURE 1. Panel (a) shows the stress-free bulk materials, with lattice parameter $a_l < a_s$ smaller (GaAsP), and larger $a_l > a_s$ (InGaAs) than that of the substrate [22]. Panel (b) illustrates a schematic representation of a pseudomorphic grown process for a layered heterostructure [18]. The material GaAsP is under a tensile strain, while the material (InGaAs) is under compressive strain, as they both are forced to conform the buffer's lattice constant a_s of a suitable semiconductor wafer.

is no longer valid and the mixing effects appear. Such phenomenology is a typical non-linear κ_{T} effect, whose most striking consequence is the predicted interchange of functions between QW and QB [12, 14]. Past theoretical studies have emphasized the existence of energy shifted bound states under κ_{T}-dependent V_{eff} [15] and a larger reduction for V_{eff} as a function of κ_{T} for light holes (*lh*) in respect to that of heavy holes (*hh*) [16]. These former works [5, 12, 14–16], were motivating enough and put us on an effort to develop a more comprehensive vision, of how V_{eff} evolves spatially with κ_{T} and strain for *hh* and *lh*. This paper is devoted to demonstrate, that V_{eff} profile evolution, QB-QW permutations and bandgap changes, are reliable tools for tuning the response threshold of a layered semiconductor system with spatial-dependent effective mass, and that VB-mixing and stress effects are possible concurrent mechanisms.

Built-in elastic strained layered heterostructures, has been remarkably used in the last decade, for development of light-emitting diodes, lasers, solar cells and photodetectors [17]. Besides, internal strain may results into a considerable modification of the electronic structure of both electrons and holes, thereby altering the response of strained systems respect to nominal behavior of strain-free designs [17]. To account for strain in the present study, we additionally suppose a heterostructure sandwiched into an arbitrary configuration of pseudomorphically strained sequence of QW-acting and QB-acting binary(ternary) alloys. This assumption is motivated by actual technological interest on specific materials and configurations. On a layer-by-layer deposition, whenever the epitaxially grown layer's lattice parameter matches that of the substrate in the in-plane direction –without collateral dislocations or vacancies– the process is referred as pseudomorphic [see Fig. 1(b)] [18]. The last one is standardized and chosen for most day-to-day applications like write-read platforms, such as sound/image players and data-manipulating devices. Our motivation arises from the probable existence of a competitor mechanism able to diminish the effects of VB-mixing on V_{eff} [13], or even wipe them out occasionally. Such prediction is not available yet in the specialized literature. The uncommon simultaneous treatment of the strain in the presence of hole-coupling effects remains absent or insufficiently addressed, thereof the scientific merit of the present theoretical attempt regarding earlier specialized reports [4, 6–8, 11, 13] is warranted.

The outline for this paper is the following: Sec. 2 presents briefly the theoretical framework to quote the VB V_{eff} for both unstressed and stressed systems. Graphical simulations on V_{eff} evolution, are exposed in Sec. 3. In that section, we discuss highly specialized III-V semiconductor binary (ternary)-compound cases with straight links to real-word technological applications. That section supports the main contribution of the present study and suggests possible applications. Sec. 4, contains the conclusions.

2. Calculation of the effective potential

Commonly, a wide class of solid-state physics problems, related to electronic and transport properties, demands the solution of multiband-coupled differential system of equations, widely known as Sturm-Liouville matrix generalized boundary problem [14]:

$$\frac{d}{dz}\left[\boldsymbol{B}(z)\frac{d\boldsymbol{F}(z)}{dz}+\boldsymbol{P}(z)\boldsymbol{F}(z)\right] + \boldsymbol{Y}(z)\frac{d\boldsymbol{F}(z)}{dz}+\boldsymbol{W}(z)\boldsymbol{F}(z)=\boldsymbol{O}_{\text{N}}, \quad (1)$$

where $\boldsymbol{B}(z)$ and $\boldsymbol{W}(z)$ are, in general, $(N\times N)$ Hermitian matrices and is fulfilled $\boldsymbol{Y}(z)=-\boldsymbol{P}^{\dagger}(z)$. In the absence of external fields, standard plane-wave solutions are assumed and it is straightforward to derive a non-linear algebraic problem

$$\boldsymbol{Q}(k_z)\boldsymbol{\Gamma}=\left\{k_z^2\boldsymbol{\mathcal{M}}+k_z\,\boldsymbol{\mathcal{C}}+\boldsymbol{\mathcal{K}}\right\}\boldsymbol{\Gamma}=\boldsymbol{O}_{\text{N}}, \quad (2)$$

called as quadratic eigenvalue problem (QEP) [16], since $\boldsymbol{Q}(k_z)$ is a second-degree matrix polynomial on the z-component wavevector k_z. In the specific case of the well-known (4×4) Kohn-Lüttinger (KL) model Hamiltonian, the matrix coefficients of equation (2) bear a simple relation with those in (1) [16]:

$$\boldsymbol{\mathcal{M}}=-\boldsymbol{B},\ \ \boldsymbol{\mathcal{C}}=2i\boldsymbol{P}\ \text{ and }\ \boldsymbol{\mathcal{K}}=\boldsymbol{W}. \quad (3)$$

Then for (4×4) KL model, the matrix coefficients of (2) can be cast as:

$$\boldsymbol{\mathcal{M}}=\begin{pmatrix} -m_{hh}^{*} & 0 & 0 & 0\\ 0 & -m_{lh}^{*} & 0 & 0\\ 0 & 0 & -m_{h}^{*} & 0\\ 0 & 0 & 0 & -m_{hh}^{*}\end{pmatrix} \quad (4)$$

$$\boldsymbol{\mathcal{C}}=\begin{pmatrix} 0 & 0 & h_{13}+iH_{13} & 0\\ 0 & 0 & 0 & -h_{13}-iH_{13}\\ h_{13}-iH_{13} & 0 & 0 & 0\\ 0 & -h_{13}+iH_{13} & 0 & 0\end{pmatrix} \quad (5)$$

$$\boldsymbol{\mathcal{K}}=\begin{pmatrix} a_1 & h_{12}+iH_{12} & 0 & 0\\ h_{12}-iH_{12} & a_2 & 0 & 0\\ 0 & 0 & a_2 & h_{12}+iH_{12}\\ 0 & 0 & h_{12}-iH_{12} & a_1\end{pmatrix} \quad (6)$$

Here $m_{hh,lh}^{*}$ stands for the (*hh*,*lh*) effective mass, respectively. We briefly introduce some parameters and relevant quantities (in atomic units) of the KL model: γ_i, with $i=1,2,3$ [Lüttinger semi-empirical VB parameters]; R [Rhydberg constant]; a_0 [Bohr radius]; E [Energy of incident and uncoupled propagating modes]; $A_{1,2}=a_0^2R\,(\gamma_1\pm\gamma_2)$, $a_{1,2}{=}A_{1,2}\kappa_{\text{T}}^2+V(z)-E$; $h_{12}{=}a_0^2R\sqrt{3}\gamma_2\left(k_y^2-k_x^2\right)$; $h_{13}{=}-a_0^2R\sqrt{3}\gamma_3k_x$; $H_{13}{=}a_0^2R\sqrt{3}\gamma_3k_y$ and $H_{12}{=}a_0^2R2\sqrt{3}\gamma_3k_xk_y$.

Bearing direct association to the original matrix dynamic equation, we exclusively focus to the case when $\boldsymbol{\mathcal{M}}$, $\boldsymbol{\mathcal{C}}$ and $\boldsymbol{\mathcal{K}}$ are constant-by-layer, hermitian, and $\boldsymbol{\mathcal{M}}$ is non-singular; therefore k_z are all different and real (symmetric) or arise in conjugated pairs (k_z,k_z^{*}). Hereafter $\boldsymbol{O}_{\text{N}}/\boldsymbol{I}_{\text{N}}$, stand for $(N\times N)$ null/identity matrix. The QEP's solutions result in the eigenvalues k_{z_j} and the eigenvectors $\boldsymbol{\Gamma}_j$. As $\boldsymbol{Q}(k_z)$ is regular, eight finite-real or complex-conjugated pairs of eigenvalues are expected. In the framework of the QEP method [16, 19], one has

$$\det\left[\boldsymbol{Q}(k_z)\right]=q_0k_z^8+q_1k_z^6+q_2k_z^4+q_3k_z^2+q_4, \quad (7)$$

is an eighth-degree polynomial with only even power of k_z and real coefficients. The coefficients q_i are functions of the system's parameters, and $q_0=\det\boldsymbol{\mathcal{M}}$ as expected [19]. In the specific case of the KL model Hamiltonian [16], q_i contain the values of γ_i and the components of the in-plane quasi-wave vector $\vec{\kappa}_{\text{T}}=k_x\widehat{e}_x+k_y\widehat{e}_y$.

Based on our procedure [19], it is straightforward to know whereas k_z is oscillatory or not by dealing with (7), and thereof to retrieve the phenomenological characteristics for V_{eff}. To manage complex-valued eigensolutions for (7) as a function of the VB-mixing and strain, we retrieve the *root-locus-like* procedure [13], provided its robustness when pursuing a simple graphical interpretation for a non-linear eigenvalue problem (2). To our knowledge, just few pure theoretical or numerical applications of the *root-locus-like* algorithm, particularly for the QEP scenario, have been previously addressed to explicitly describe several standard III-V semiconductor compounds [13, 19]. We acknowledge the advantages of the *root-locus-like* technique application within the low-dimensional solid state physics [13, 19] –we may be the first ones– and try to predict unknown phenomenology whenever coupled holes interplay with mutable V_{eff} of the stressed system. For some high specialized zinc-blenda and wurtzite systems, current knowledge of the hole quantum transport mechanism is limited. The present theoretical contribution, claims to shed light on that issue. We think readers will be interested more on how the V_{eff} metamorphosis under VB-mixing and strain could influence their real-world devices, rather than getting involved into the very details of the theoretical

model itself. In regard to that concern, we propose a simple and comprehensive modelling procedure for $V_{\rm eff}$ to deal with, and a *gedanken*-like simulation for a passage of mixed holes throughout a strained-free and strained layered heterostructures. The purpose of that is hardly a hypothetic exercise, but rather pretends to show to condensed-matter theoreticians and to complementary-fields physicists, why a non-mutable $V_{\rm eff}$ under VB-mixing and strain is not acceptable and how they can re-model $V_{\rm eff}$ to improve their own works within similar conditions.

According to prior description for VB-mixing [5] and in order to achieve the target of the present study, an effective potential operator $\widehat{\boldsymbol{W}}_{\rm eff}$ has to be put together, which in our modelling implies to select every spatial configuration-dependent function from Hamiltonian (1) [12,16]. By choosing the first-quantization axis, that of the z-coordinate direction [along the heterostructure growth seen in Fig. 1(b)], we are required not to consider terms from (1), counting as part of their arguments the k_z-component of $\vec{\kappa}_{\rm T}$, then

$$\widehat{\boldsymbol{W}}_{\rm eff} = \begin{bmatrix} W_{11} & W_{12} & 0 & 0 \\ W_{12}^{*} & W_{22} & 0 & 0 \\ 0 & 0 & W_{22} & W_{12} \\ 0 & 0 & W_{12}^{*} & W_{11} \end{bmatrix}. \tag{8}$$

Next we follow symmetry considerations [20], and solve a Schrodinger-like equation in the (2×2) Hilbert reduced-space of the KL model

$$\left[\widehat{\boldsymbol{W}}_{\rm eff}^{2}(z) - V_{\rm eff}\boldsymbol{I}_2\right]\boldsymbol{\Psi}(z) = \boldsymbol{O}_2, \tag{9}$$

whose eigensolutions are the expected values for $V_{\rm eff}$. The superscript indicates the order of the corresponding matrix. The operator $\widehat{\boldsymbol{W}}_{\rm eff}$ was previously proposed elsewhere for an unstressed system [13] and being approximately correct, although not accurate, is reliable enough to simulate the evolution of $V_{\rm eff}$ under the envisioned scenarios. We have taken $W_{11(22)} = A_{1(2)}\kappa_{\rm T}^2 + V(z)$ and $W_{12} = (\hbar^2\sqrt{3}/2\,m_0)\left(\gamma_2(k_y^2 - k_x^2) + 2i\gamma_3 k_x k_y\right)$, with m_0 as the bare electron mass. For $\kappa_{\rm T} \approx 0$ the VB-mixing vanishes, thereby $\boldsymbol{V}(z) = V_{\rm B} - V_{\rm A} = \Theta V_{\rm eff}$, is a positive-valued constant functional step-modulated by Θ, where $V_{\rm A/B}$ stands for the potential of the concomitant materials A/B, respectively [see Fig. 1(a)]. Due the lack of a strict superlattice multiple-layered structures under study here, we have neglected the spontaneous in-layer polarization field for III-nitride constituent media [21], thus assuming a rectangular potential profile as test-run input, rather than biased one for all III-nitride slabs of the heterostructures. As the III-nitride slabs are just a few, we mean the intrinsic-biased-profile variation to be small over the unit cell, thus negligible for the heterostructure.

Strain field may rise questions over their relative effects on the electronic structure and, in particular on the valence-band structure where shape and size of the potential profile lead to stronger hybridization of the quantum states. Lets now examine the effects of the stress in the framework of the KL model Hamiltonian. The existence of a biaxial stress applied upon the plane parallel to the heterostructure interfaces leads to the appearance of an in-plane strain. The effective potential operator $\widehat{\boldsymbol{W}}_{\rm eff}$ in the presence of biaxial strain, can be written as [22]

$$\widehat{\widehat{\boldsymbol{W}}}_{\rm eff}^{2}(z) = \widehat{\boldsymbol{W}}_{\rm eff}^{2}(z) + U_s\boldsymbol{I}_2, \tag{10}$$

where

$$U_s = -\left\{a_v(2\varepsilon_1 + \varepsilon_3) + b(\varepsilon_1 - \varepsilon_3)\right\}, \tag{11}$$

is the accumulated strain energy resulting from the tensile or compressive stress acting on the crystal, when an epitaxial layer is grown on a different lattice-parameter substrate. Owing to strictness in formulation [22], we guess that a maximum-quota criterium (11) suffices to achieve the goal posted in Sec. 1. Being independent from $\kappa_{\rm T}$, a maximized U_s was taken for granted to evaluate if there is a real challenger strain effect over VB-mixing's influence on the metamorphosis of $V_{\rm eff}$. In (10)-(11), the subscript s stands for strain. In (11) a_v/b represent the Pikus-Bir deformation/break potentials, describing the influence of hydrostatic/uniaxial strain. Meanwhile $\varepsilon_{1,3}$, are the *in-plane*, and *normal-to-plane* lattice displacements, respectively. For commonly used cubic and hexagonal semiconductor compounds, we assume [17,18]

$$\varepsilon_1 = -\frac{a_s - a_l}{a_l} \tag{12}$$

with $a_{s,l}$ the lattice parameter of the substrate and the epitaxial layer, respectively. Though no external stress is considered along the growth direction z, the lattice parameter is forced to change due to the Poisson effect [18]. Hence, the normal-to-plane displacement can be cast as

$$\varepsilon_3 = -\nu\,\varepsilon_1, \tag{13}$$

which remains connected to in-plane deformation ε_1 *via* the Poisson radio ν. The last is valid for zinc blende and wurtzite materials.

By changing the material and the growth plane, the value of ν modifies. For cubic materials it reads [17]

$$\nu_{\rm cub} = \begin{cases} 2\frac{C_{12}}{C_{11}} & \text{for growth plane: } (001) \\ \frac{C_{11}+3C_{12}-2C_{44}}{C_{11}+C_{12}+2C_{44}} & \text{for growth plane: } (110) \\ \frac{2(C_{11}+2C_{12}-2C_{44})}{C_{11}+2C_{12}+4C_{44}} & \text{for growth plane: } (111) \end{cases}, \tag{14}$$

while for the hexagonal ones we have [17]

$$\nu_{hex} = \begin{cases} 2\frac{C_{13}}{C_{33}} & \text{for growth plane: } (0001) \\ \frac{C_{12}\varepsilon_1+C_{13}\varepsilon_c}{C_{11}} & \text{for growth plane: } (1\bar{1}00) \\ \frac{C_{12}\varepsilon_1+C_{13}\varepsilon_c}{C_{11}} & \text{for growth plane: } (1\bar{1}02) \end{cases}. \tag{15}$$

To quote the parameter $\varepsilon_c = ((c_s - c_l)/c_l)$, we take c_s from the substrate wafer [23], while c_l is referred to the epitaxially-grown layer on buffer stratum.

For the sake of completeness of the present theoretical framework, we have derived analytic expressions for the VB-*band offset* $V_{\rm eff}$ as a straightforward function of the band mixing parameters and the strain energy. In current solid-state physics studies, the later could allow a comprehensive analysis in cubic as well as in hexagonal layered-stressed semiconductor systems, whenever one manages to manipulate the accumulated pseudomorphic strain and mixing effects in a single shoot. We have considered (10)-(11) for solving (9), and thus for zinc blende (cubic) materials it may be cast

$$V_{\rm eff}^{lh,hh} = \Delta U_s + \Delta V(z) - \Delta E + Ra_0{}^2\left[\pm\xi_B \mp \xi_A + \kappa_{\rm T}{}^2\left(-\gamma_1^{\rm A} + \gamma_1^{\rm B}\right)\right], \quad (16)$$

being

$$\Delta E = E^{\rm B} - E^{\rm A}; \quad \Delta U_s = U_s^{\rm B} - U_s^{\rm A}; \quad \Delta V(z) = V_z^{\rm B} - V_z^{\rm A}$$

and

$$\xi_j = \sqrt{\left(\gamma_2^j\right)^2 \kappa_{\rm T}^4 + 3\left(\gamma_2^j\right)^2 k_x{}^4 - 6\left[\left(\gamma_2^j\right)^2 k_x{}^2 k_y{}^2\right] + 3\left[\left(\gamma_2^j\right)^2 k_y{}^4\right] + 12\left[\left(\gamma_3^j\right)^2 k_x{}^2 k_y{}^2\right]},$$

for $j = A, B$. In these expressions, E^j stands for the particle energy in the material j; while U_s^j represents the accumulated pseudomorphic strain energy due the substrate-material stress concerning each layer j independently and finally V_z^j refers to QW-acting or QB-acting potentials, whenever the slab j plays one or the other role in the heterostructure. Worthwhile to remark the clear parabolic dependence of $V_{\rm eff}^{lh,hh}$ on $\kappa_{\rm T}$ as it readily shown in (16). The later is straightforwardly confirmed in the numerical simulation of the VB-offset depicted below.

For systems that crystalize in the wurtzite structure have been derived a (6×6) effective Hamiltonian $\hat{\boldsymbol{H}}_6(k)$, within the envelope function approximation [24]. By an unitary canonical transformation $\mathbb{U}$, the original Hamiltonian is re-expressed as

$$\mathbb{U}^\dagger \hat{\boldsymbol{H}}_6(k)\mathbb{U} = \begin{pmatrix} \hat{\boldsymbol{H}}_3^{\,u} & \boldsymbol{O}_3 \\ \boldsymbol{O}_3 & \hat{\boldsymbol{H}}_3^{\,l} \end{pmatrix}, \quad (17)$$

yielding a (6×6) block-diagonal Hamiltonian, quite similar in general sense to the reduced-space KL Hamiltonian we had used for the zinc blend heterostructures. The sub-scripts $u(l)$ stand for up(low) respectively, as a resemblance of the up(down) spin-electronic states flavors and have been introduced by Broido and Sham [25], who found alike transformation as (17), but for the (4×4) KL model. The (3×3) Hilbert reduced-space blocks in (17), satisfy the following symmetry relation

$$\hat{\boldsymbol{H}}_3^{\,l} = \left(\hat{\boldsymbol{H}}_3^{\,u}\right)^*, \quad (18)$$

which is an analog to that deduced for the (2×2) Hilbert reduced-space of the KL model [20]. Preserving the same conception framework posted above, the potential-energy operator $\widehat{\boldsymbol{W}}_{\rm eff}^{\,6}(z)$ for the wurtzite along the quantization axis z, is obtained by discarding all elements associated to the z-component wavevector k_z. In doing that, we assume understood the implications of the translational invariance symmetry in the $[xy]$ plane. Thereof

$$\widehat{\boldsymbol{W}}_{\rm eff}^{\,6}(z) = \begin{pmatrix} \widehat{\boldsymbol{W}}_3^{\,u} & \boldsymbol{O}_3 \\ \boldsymbol{O}_3 & \widehat{\boldsymbol{W}}_3^{\,l} \end{pmatrix}, \quad (19)$$

whose blocks fulfil

$$\widehat{\boldsymbol{W}}_3^{\,l} = \left(\widehat{\boldsymbol{W}}_3^{\,u}\right)^*. \quad (20)$$

The up-block of (19) –in the presence of biaxial pseudomorphic strain–, has the general form

$$\widehat{\widehat{\boldsymbol{W}}}_3^{\,u} = \begin{pmatrix} \widehat{\widehat{W}}_{11}^{\,u} & \widehat{\widehat{W}}_{12}^{\,u} & 0 \\ \widehat{\widehat{W}}_{12}^{\,u} & \widehat{\widehat{W}}_{22}^{\,u} & \widehat{W}_{23}^{u} \\ 0 & \left(\widehat{\widehat{W}}_{23}^{\,u}\right)^\dagger & \widehat{\widehat{W}}_{33}^{\,u} \end{pmatrix}, \quad (21)$$

while its matrix elements are taken as

$$\widehat{\widehat{W}}_{11}^{\,u} = F_o + \frac{\hbar^2}{2m_o}\mathcal{A}_2\kappa_{\rm T}^2 + V(z) + U_s;$$

$$\widehat{\widehat{W}}_{12}^{\,u} = \frac{\hbar^2}{2m_o}\mathcal{A}_5\kappa_{\rm T}^2;$$

$$\widehat{\widehat{W}}_{22}^{\,u} = G_o + \frac{\hbar^2}{2m_o}\mathcal{A}_2\kappa_{\rm T}^2 + V(z) + U_s;$$

$$\widehat{\widehat{W}}_{23}^{\,u} = \frac{\sqrt{2}}{3}\Delta_{so}^{\perp};$$

$$\left(\widehat{\widehat{W}}_{23}^{\,u}\right)^\dagger = \widehat{\widehat{W}}_{23}^{\,u} = \frac{\sqrt{2}}{3}\Delta_{so}^{\perp};$$

$$\widehat{\widehat{W}}_{33}^{\,u} = \frac{\hbar^2}{2m_o}\mathcal{A}_2\kappa_{\rm T}^2 + V(z) + U_s;$$

together with $F_o(G_o)$=$\Delta_1 \pm \Delta_2$; $\mathcal{A}_2$=$1 - 6\pi_z$; $\mathcal{A}_5 = -3\sigma$; and $\Delta_2 = (1/3)\Delta_{so}^z$. Owing to brevity we re-address readers to a more detailed description for matrix elements of the

Hamiltonian $\hat{\boldsymbol{H}}_6(k)$ and thereof for (21), which have been accurately focused previously [24]. However, worthwhile comment here that: Δ_1 represents the energy splitting produced by the anisotropy of the hexagonal symmetry; $\mathcal{A}_{2,5}$ enter as some material dependent semi-empiric band parameters, and $\Delta_{so}^{z,\perp}$ quote the energy splitting in the z-direction (perpendicular to it), due to the spin-orbit (so) interaction.

On the ground of symmetry relations (18) and (20), the quoting of $\widehat{\boldsymbol{W}}^{6}_{\rm eff}(z)$ *eigen*-solutions *via* (9), becomes a suitable task. However, for the purposes posted in the present study it suffices to figure it out the same but for $\widehat{\boldsymbol{W}}^{u}_{3}$, whose third-order characteristic polynomial equation reads

$$(\omega^u)^3 + \alpha\,(\omega^u)^2 + \beta\omega^u + \delta = 0, \tag{22}$$

and has the solutions

$$\omega^u = \begin{cases} -\frac{1}{3}\left[\alpha + \eta + \zeta_o\eta^{-1}\right] & \text{for split-off holes} \\ \frac{1}{3}\left[\alpha + \rho\eta + \zeta_o(\rho\eta)^{-1}\right] \\ -\frac{1}{3}\left[\alpha + \rho^*\eta + \zeta_o(\rho^*\eta)^{-1}\right] \end{cases}. \tag{23}$$

For (22) and (23) we have taken

$$\alpha = -tr\left\{\widehat{\widehat{\boldsymbol{W}}}^{u}_{3}\right\};$$

$$\beta = -(\widehat{\widehat{W}}^{u}_{12})^2 - (\widehat{W}^{u}_{23})^2 + \widehat{\widehat{W}}^{u}_{11}\widehat{\widehat{W}}^{u}_{22} + \widehat{\widehat{W}}^{u}_{11}\widehat{\widehat{W}}^{u}_{33} + \widehat{\widehat{W}}^{u}_{22}\widehat{\widehat{W}}^{u}_{33};$$

$$\delta = \widehat{\widehat{W}}^{u}_{33}(\widehat{\widehat{W}}^{u}_{12})^2 + \widehat{\widehat{W}}^{u}_{11}(\widehat{\widehat{W}}^{u}_{23})^2 - \widehat{\widehat{W}}^{u}_{11}\widehat{\widehat{W}}^{u}_{22}\widehat{\widehat{W}}^{u}_{33};$$

$$\rho = \frac{1}{2}(-1 + i\sqrt{3});$$

$$\eta = \sqrt[3]{\frac{\zeta_1 + \sqrt{\zeta_1^2 - 4\zeta_o^3}}{2}};$$

$$\zeta_o = \alpha^2 - 3\beta;$$

$$\zeta_1 = 2\alpha^3 - 9\alpha\beta + 27\delta.$$

3. Discussion of results

Unless otherwise specified, the graphical simulations of $V_{\rm eff}$ reported here, were calculated using highly specialized III-V semiconductor binary(ternary)-compound cases for both unstressed and stressed cubic and hexagonal systems. The present numerical simulations consider different constituent media, regardless if they can be grown. In this section, we briefly present numerical exercises within the *root-locus-like* technique, to foretell multiband-coupled charge-carrier effects for pseudomorphically stressed III-V semiconductor layered systems.

3.1. Simulation of $V_{\rm eff}$ profile evolution

On general grounds, for $\kappa_{\rm T} \approx 0$ the $V_{\rm eff}$ is constant [14, 16], while by letting grow $\kappa_{\rm T}$, the band mixing effects arise and $V_{\rm eff}$ changes [12, 14, 16]. We are focused here on evaluating first the stress-free systems, and then the effect of a pseudomorphic strain on $V_{\rm eff}$.

3.1.1. Unstressed $V_{\rm eff}$ metamorphosis

Pursuing a deeper understanding of the rather cumbersome $\kappa_{\rm T}$ impact over the $V_{\rm eff}$, we simulate its profile evolution for pure ($\kappa_{\rm T} \approx 0$) and mixed ($\kappa_{\rm T} \neq 0$) holes. To get this problem solved, one has to figure out (9) for several III-V semiconducting heterostructures, having taken external layers length as 25 Å and the embedded stripe thickness as 50 Å.

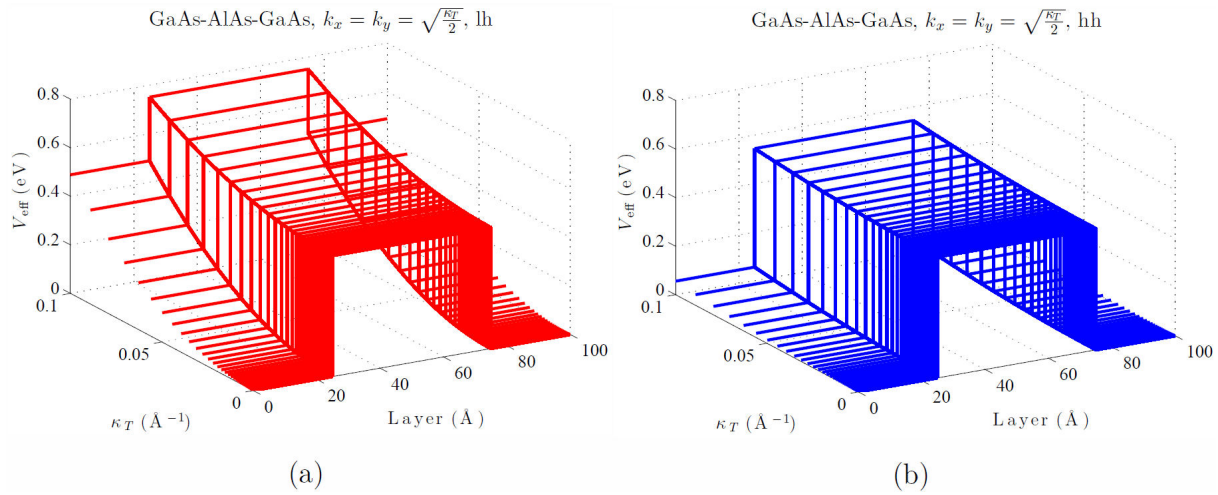

FIGURE 2. (Color online) Panel (a)/(b) displays the metamorphosis of the effective potential profile $V_{\rm eff}$ for *lh*/*hh* (red/blue lines), as a function of $\kappa_{\rm T}$ and layer dimension for a GaAs/AlAs/GaAs heterostructure.

Figure 2 confirms the fixed-height V_z as a reliable input QB-energy for *hh* (blue lines), valid even for a strong VB-mixing [see panel (b)]. The opposite reveals panel (a) for *lh* (red lines), considering the V_z trend to diminish with κ_{T}. This kind of evidence suffices to demonstrate the essentialness of introducing a mutable effective *band offset* V_{eff}, to correctly characterize scattering processes for holes. There are further features that deserve to be referred, indeed: the left(right) V_{eff} edges move upward non-rigidly nearly 0.5 eV, meanwhile middle border stays practically unchangeable. Worthwhile to remark that we recovered here a phenomenology of this sort, previously obtained for the first bound states of *lh* and *hh* in a QW [26]. We had found the same behavior of the embedded layer for other materials of real-word interest (*AlSb*, *AlP*, *AlN*).

An appealing situation arises at a specific entry of the transverse momentum. An earlier detailed study on this subject [12], has predicted the existence of quantity $\kappa^2_{\text{To}} = 2V_o m^{\text{A}} m^{\text{B}} \left[\hbar^2 \left(m^{\text{B}} - m^{\text{A}}\right)\right]$, for which V_{eff} becomes constant along the entire layered heterostructure. In the case envisioned here, due to the presence of *hh* and *lh*, we have

$$\kappa^2_{\text{To}(hh,lh)} = \frac{2V_o m_o^3 \hbar^2}{\left(\gamma_1^{\text{A}} \mp 2\gamma_2^{\text{A}}\right)\left(\gamma_1^{\text{B}} \mp 2\gamma_2^{\text{B}}\right)} \times \left[\frac{1}{\left(\gamma_1^{\text{B}} \mp 2\gamma_2^{\text{B}}\right)} - \frac{1}{\left(\gamma_1^{\text{A}} \mp 2\gamma_2^{\text{A}}\right)}\right], \qquad (24)$$

being $V_o = V_{\text{eff}}(\kappa_{\text{T}} = 0)$, and A/B standing for concomitant cladding/middle layer. A direct consequence for V_{eff} being flat at κ_{To} is the existence of a crossover of V_{eff} respect to (24).

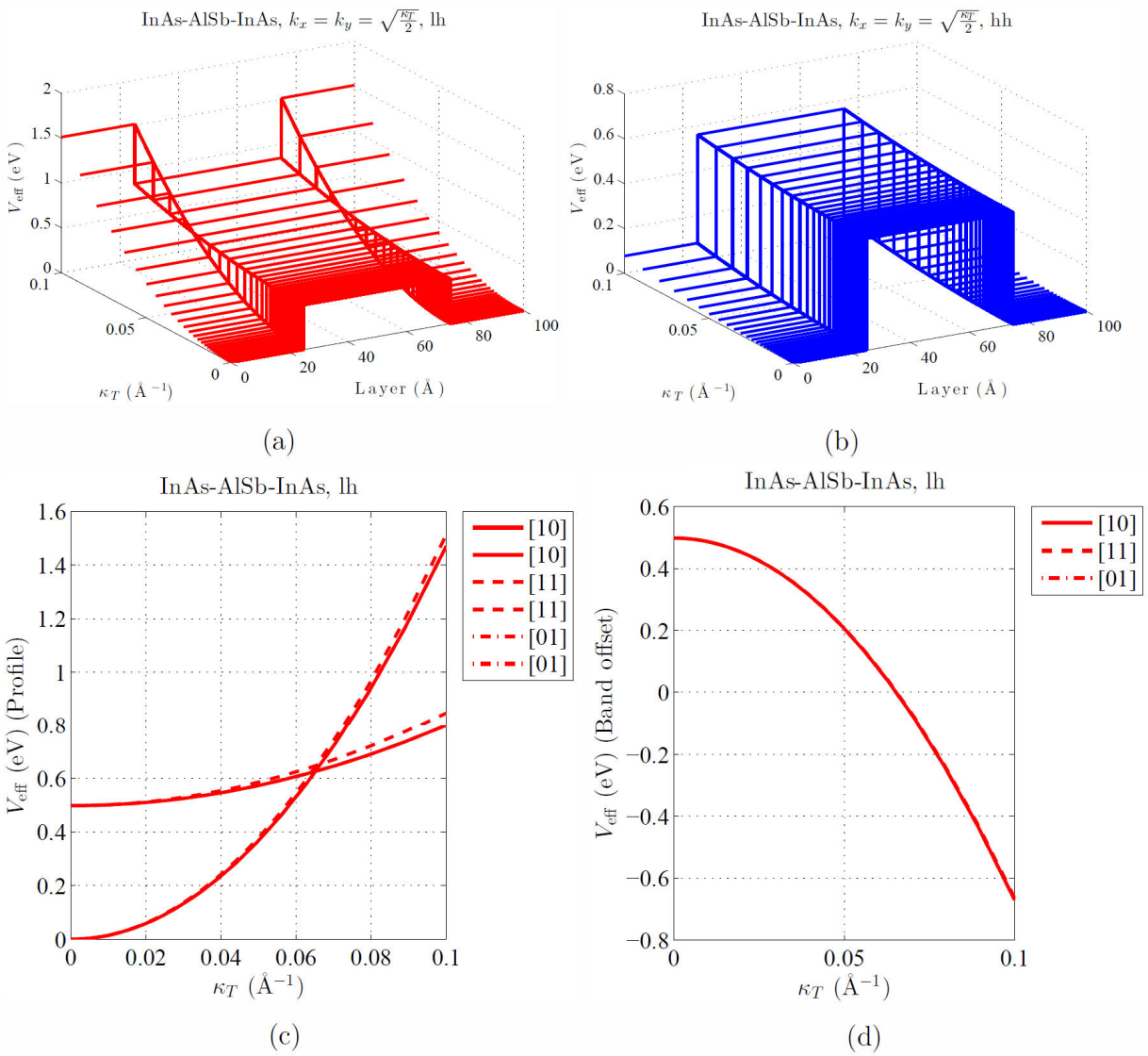

FIGURE 3. (Color online) Panel (a)/(b) displays the $3D$-perspective evolution of the V_{eff} profile for *lh*/*hh* (red/blue lines), as κ_{T} and layer dimension grow. Panel (c) displays a cut of the V_{eff} profile for *lh* (red line), at the interface plane between left and middle layers, as a function of κ_{T}. Panel (d) shows the progression of the *band offset*, at the same interface for *lh*, *i.e.* the difference between the upper-edge and lower-edge of the V_{eff} profile. We have considered a InAs/AlSb/InAs stress-free layered heterostructure.

In other words, if a QW-like profile is present for $\kappa^2_{\text{T}(hh,lh)} < \kappa^2_{\text{To}(hh,lh)}$, then a QB-like profile appears at $\kappa^2_{\text{T}(hh,lh)} > \kappa^2_{\text{To}(hh,lh)}$, or the other way around.

In Fig. 3(a) the V_{eff} valence-band mixing dependence, exhibits a neatly permutation of the V_{eff} character as the one predicted for electrons [12]. This permutation pattern is what we call "*keyboard*" effect, and was detected for *lh* only in stress-free systems. This striking interchange of roles for QB-like and QW-like layers, whenever the in-plane kinetic energy, varies from low to large intensity, represents the most striking contribution to the present study. For a single-band-electron Schrödinger problem, some authors have predicted that both QW and QB may appear in the embedded layers of a semiconductor superlattice, depending on the transverse-component value of the wave vector [12]. It has recently been unambiguously demonstrated that the effective-*band offset* energy V_{eff}, "*felt*" by the two flavors of holes, as κ_{T} grows, is not the same. Inspired by these earlier results, we have addressed a wider analysis of this appealing topic, displayed in Fig. 3, pursuing a more detailed insight. We have considered a InAs/AlSb/InAs heterostructure. Panel (a)/(b) of Fig. 3 shows explicitly the metamorphosis of V_{eff}, felt by both flavors of holes independently, respect to concomitant-material slabs. From panels (a) and (b), it is straightforward to see that for *hh* (blue lines) an almost constant V_{eff} remains, while κ_{T} varies from 0 (uncoupled holes) to 0.1 Å^{-1} (strong hole band mixing), despite the respective band-edge levels have changed. Contrary to *hh* [blue lines, panel (b)], the *lh* exclusively [red lines, panel (a)] exhibit the *keyboard* effect, *i.e.* they feel an effective *band offset* exchanging from a QW-like into a QB-like one, and *viceversa* for an InAs/AlSb/InAs heterostructure while κ_{T} increases. The evident *keyboard* effect

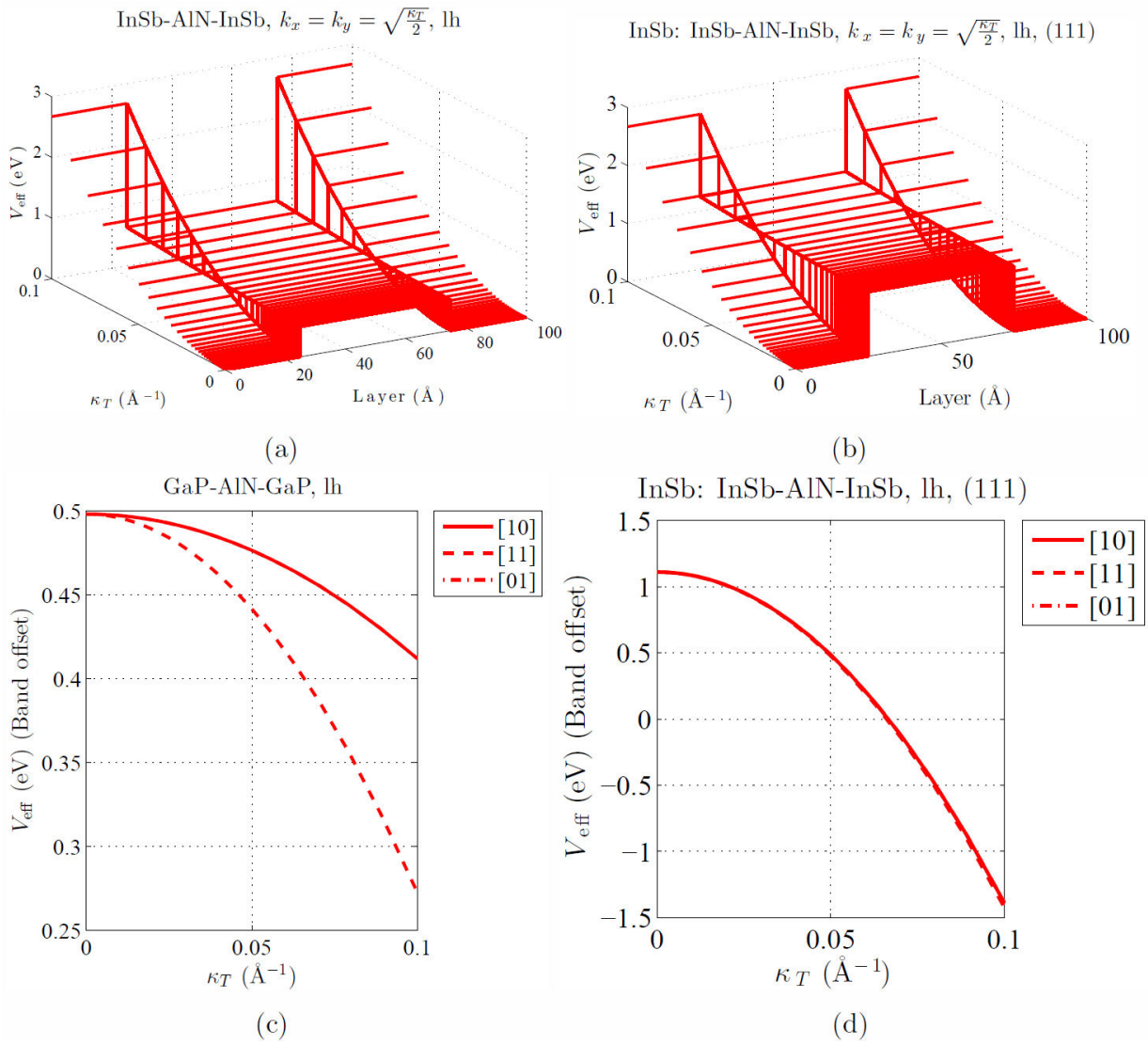

FIGURE 4. (Color online) Panel (a) displays the $3D$-perspective evolution of the stress-free V_{eff} profile for *lh* as κ_{T} and layer dimension grow. Panel (b) shows the same for a InSb:InSb/AlN/InSb strained layered heterostructure. Panel (c) exhibits the evolution of the *band offset* for *lh*, in a stress-free GaP/AlN/GaP system. Panel (d) shows the same for a InSb:InSb/AlN/InSb strained heterostructure.

of V_{eff}, resembles a former prediction for electrons [12]. This observation means that in the selected rank of parameters for a given binary-compound materials, a *lh* might "*feel*" a qualitative different V_{eff} (QW or QB) during its passage through a layered system, while the degree of freedom varies in the transverse plane. Former assertions can be readily observed in Fig. 3(c)-(d), where we have plotted the evolution of V_{eff} profile [panel (c)], as well as the progression of the *band offset* [panel (d)], with κ_{T} at a fixed transverse plane of the heterostructure. Both upper-edge and lower-edge move in opposite directions [see panel (c)] and the zero-*band offset* point configuration is detected in the vicinity of $\kappa_{\text{T}} \approx 0.066$ Å^{-1} [see panel (d)]. The permutation holds for other in-plane directions, as can be seen from panel (c). Although not shown here for simplicity, the *keyboard* effect, remains robust for other middle-layer binary compounds, namely: AlAs, AlP, and AlN.

3.1.2. Keyboard effect *versus* pseudomorphic strain

Turning now to built-in elastic stressed layered heterostructures, we are interested in answering a simple question: whether or not the existence of a pseudomorphic strain becomes a weak or a strong competitor mechanism able to diminish the *keyboard* effect on V_{eff}, or even make it rises/vanishes occasionally. Thereby, we need to account the accumulated strain energy resulting from the tensile or compressive stress acting on the crystal slabs. The last requires to solve (10), assuming the heterostructure sandwiched into a pseudomorphically strained QW/QB/QW-sequence.

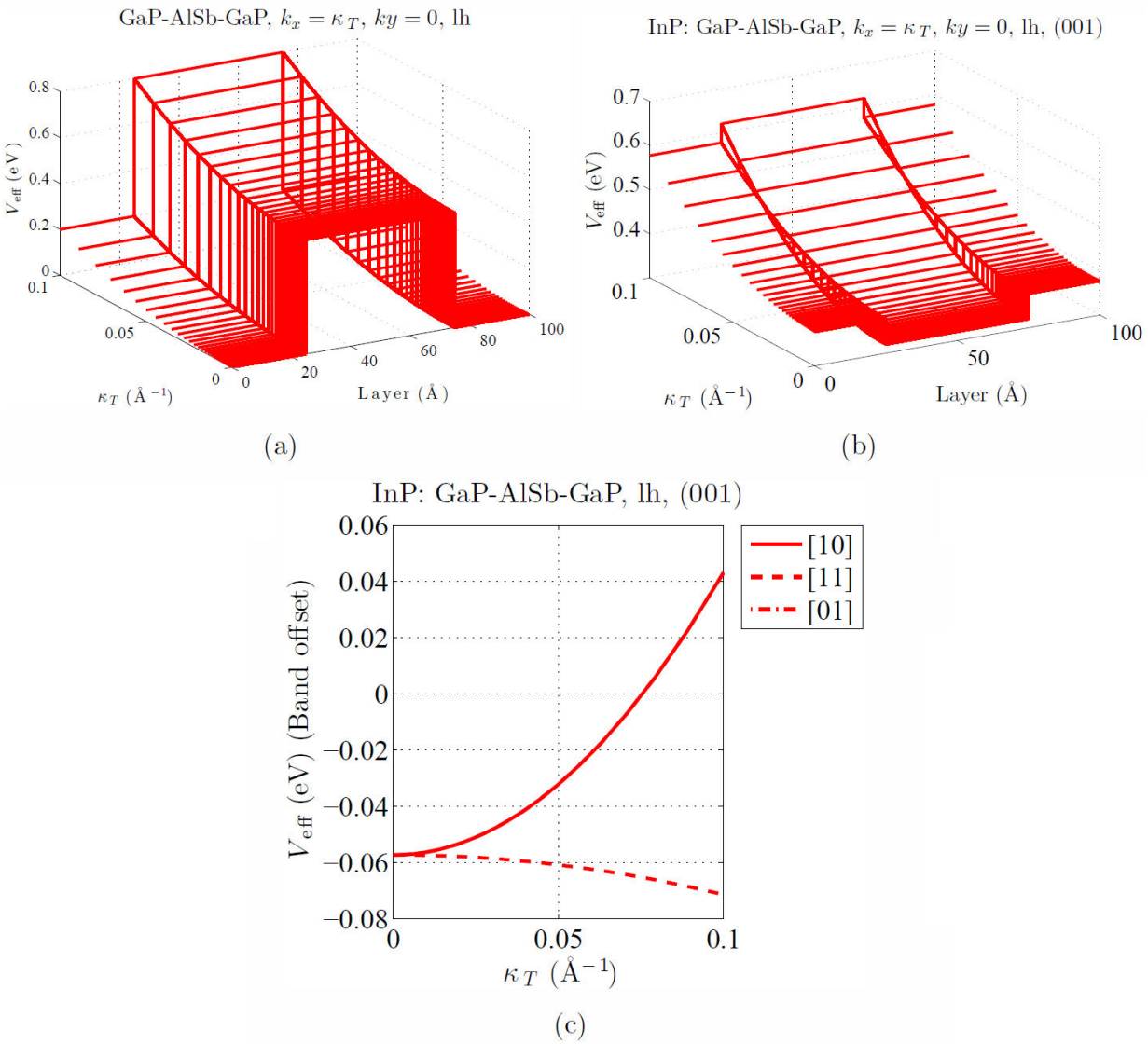

FIGURE 5. (Color online) Panel (a) displays the $3D$-perspective evolution of the stress-free V_{eff} profile for *lh* as κ_{T} and layer dimension grow. Panel (b) shows the same for a InP:GaP/AlSb/GaP strained layered heterostructure. Panel (c) plots the progression of the *band offset* for *lh*, considering a InP:GaP/AlSb/GaP strained heterostructure along several in-plane directions.

Figure 4 is devoted to demonstrate that the *keyboard* pattern for *lh* remains robust in a *InSb*:*InSb*/*AlN*/*InSb* pseudomorphically strained layered heterostructure [see panel (b)], respect to that of the stress-free system [see panel (a)]. In this case, we conclude that maximized U_s (11) do not represent any antagonist mechanism regarding to valence-band mixing influence on V_{eff}. Identical middle-layer nitride material (*AlN*) may not follow a same evolution of VB-offset, if the concomitant cladding layers change. This in shown in panel (c), whose displayed behavior is the opposite to that in panel (a), *i.e.* we found no evidences of the *keyboard* effect. In this case, none zero-*band offset* point configuration were found even at strong VB mixing, though a remarkable anisotropy was detected, despite a common trend of V_{eff} is neatly preserved. On the contrary, a robust isotropic character in the VB-offset progression for the same middle-layer binary compound embedded in the strained heterostructure, have been detected and shown in panel (d).

Figure 5(b) exhibits an unexpected *keyboard* effect for *lh* in a InP:GaP/AlSb/GaP layered heterostructure under a pseudomorphic strain, in comparison with a stress-free heterostructure [see panel (a)]. This evidence encourages to suggest U_s (11) as a trigger mechanism in the presence of valence-band mixing to influence V_{eff}, forcing a qualitative distinctive phenomenology to arise in the effective VB-offset profile (*keyboard* effect). Besides, it is worth to underline the inversion of the valence-band line-up, which is also remarkable considering the appealing interplay from QW-like to QB-like behavior (and *viceversa*) when comparing both stress-free [see panel (a)] and strained [see panel (b)] heterostructures. It is worth noticing the difference in the phenomenology of several stressed antimonide-based systems,

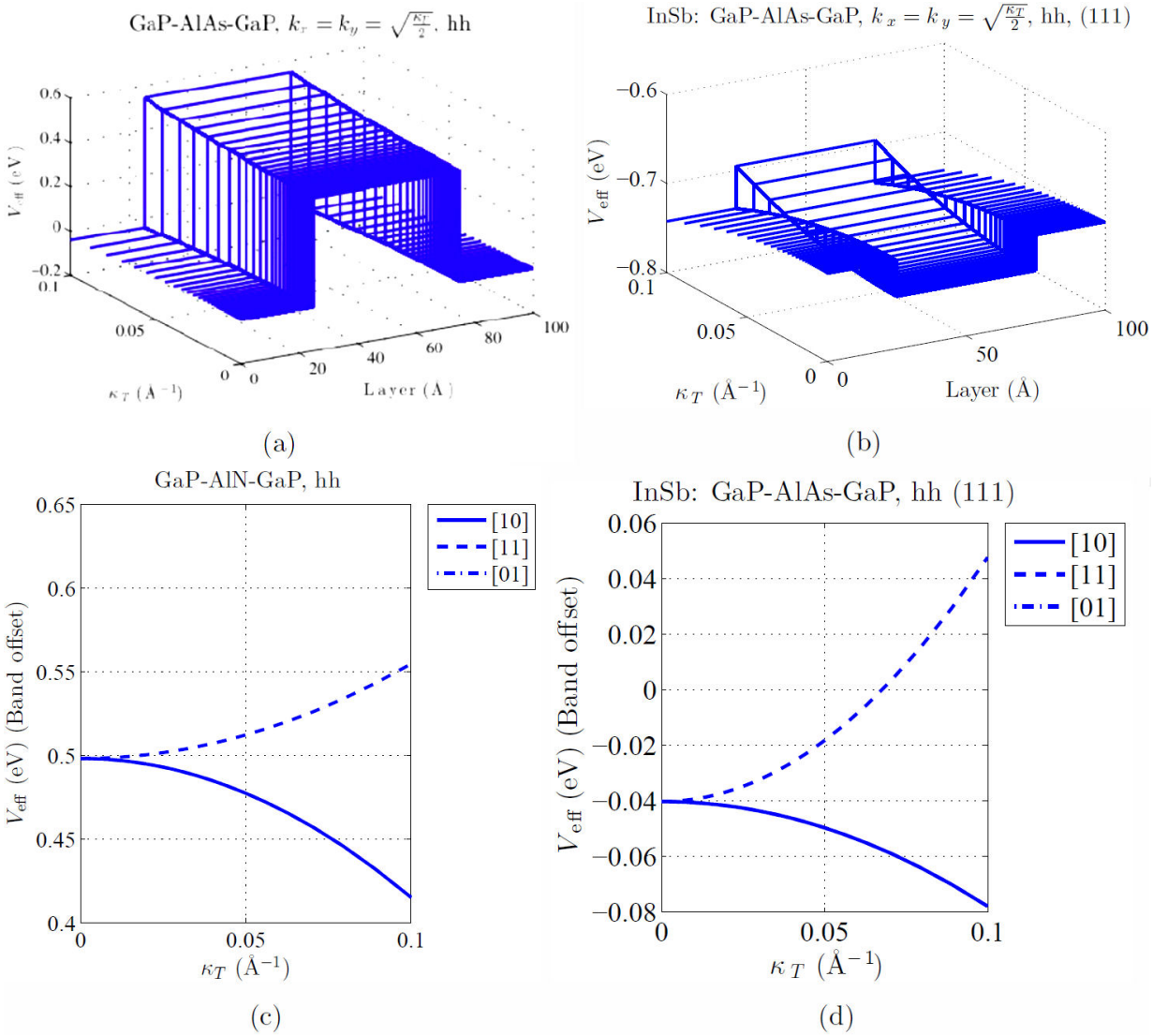

FIGURE 6. (Color online) Panel (a) shows the stress-free evolution of V_{eff} for *hh* as a function of κ_{T} and layer thickness. Panel (b) shows the same for a AlN:GaP/AlAs/GaP strained layered heterostructure. Panel (c) displays the metamorphosis of the *band offset* for *hh*, in a stress-free GaP/AlN/GaP system. Panel (d) shows the same for a InSb:GaP/AlAs/GaP strained heterostructure.

respect to that discussed for nitride ones in Fig. 4(d). As can be seen in Fig. 5(c), an anisotropic pattern characterizes the *lh* case in a InP:GaP/AlSb/GaP layered heterostructure under a pseudomorphic strain. Importantly, the *keyboard* effect on V_{eff} stays steady along [10] and [01] in-plane directions, while vanishes in the [11]. Thus a topological tuning of this striking effect reveals possible.

Figure 6 shows another striking performance of V_{eff}, when unexpectedly a *keyboard* effect has arisen for *hh* in a InSb:GaP/AlAs/GaP strained layered heterostructure [see panel (b)]. Indeed, if we consider the stress-free case of Fig. 6(a), we can see that the standard rectangular distribution for V_{eff} remains consistent in a wide range of κ_{T}. Furthermore, a valence-band line-up inversion takes place, which is yet another remarkable performance for QW-like and QB-like slabs. For the sake of continue the qualitative insight into the influence of the concomitant cladding/middle layers as presented in the discussion of Fig. 4(a,c), we alter here just the cladding ones. At the opposite to the mentioned previous case for *lh*, the same kind of V_{eff} evolution for *hh* remains [see panels (a) and (c)], however a difference of tendency along [10] and [01] in-plane directions, respect to that of the [11], was observed. We underline in panel (d), the possibility for topological tuning of the *keyboard* effect on V_{eff}, as for *hh* now the [11] in-plane direction solely shows a zero-*band offset* point at the vicinity of $\kappa_{\text{T}} \approx 0.075$ Å^{-1}.

Finally, Fig. 7 confirms the existence of a strong competitor mechanism between strain and *keyboard* effect. We can see in Fig. 7(b) how the *keyboard* pattern vanishes in a AlAs:InAs/AlN/InAs layered heterostructure under a pseudomorphic strain. The envisioned effect was apparently robust for the stress-free analogous systems shown in panel (a), within the selected range of κ_{T}. In panel (d), a resembling phenomenon was found for the strained InSb:InSb/AlAs/InSb layered heterostructure, with an appealing bonus of the interplay from QW-like to QB-like behavior (and *viceversa*) of the slabs. The last inversion of the valence-band line-up was not obtained for the stress-free correspondent system, exhibited in Fig. 7(c).

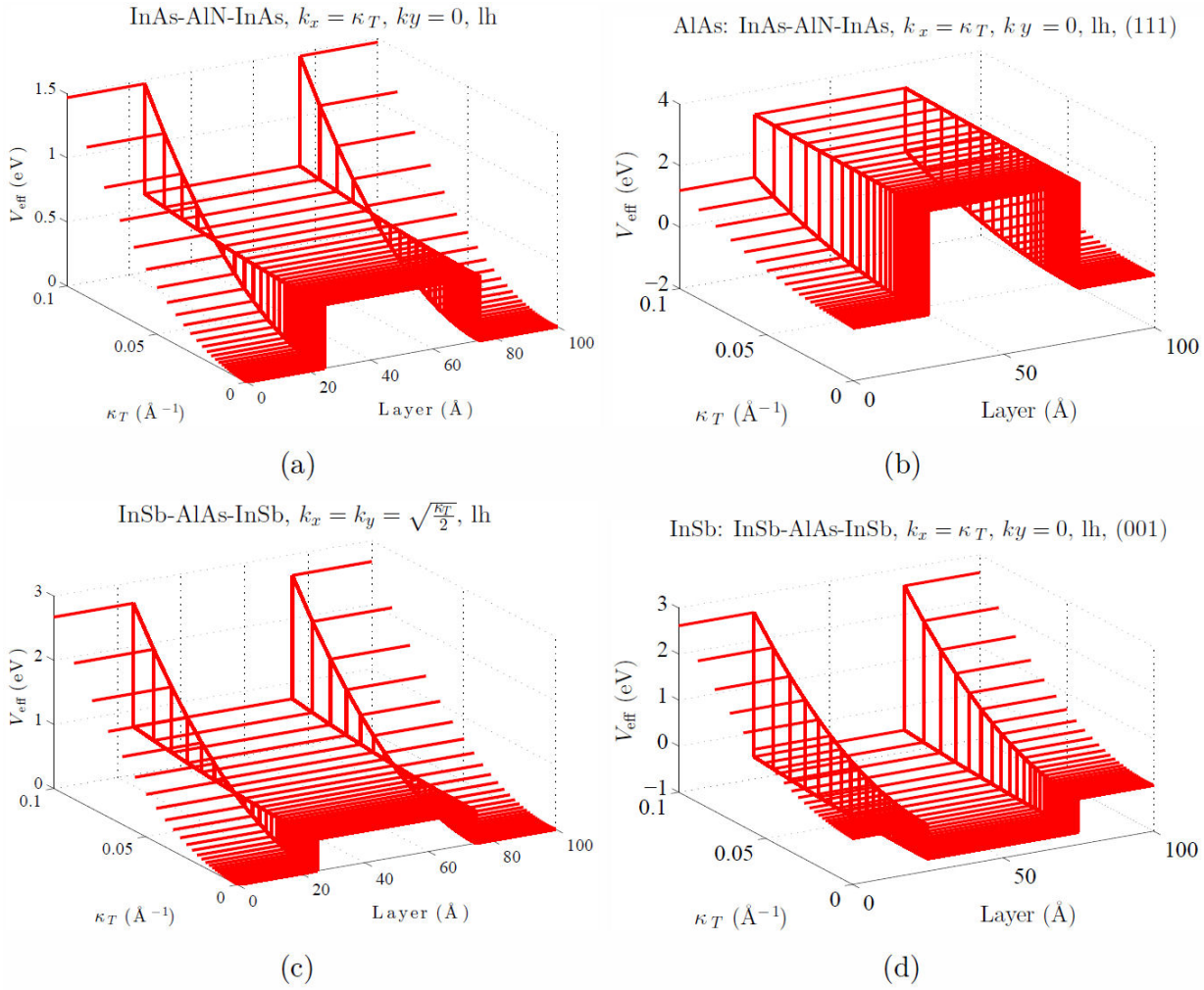

FIGURE 7. (Color online) V_{eff} profile metamorphosis of for stress-free/strained layered heterostructure (panel a,c)/(panel b,d) as κ_{T} and layer thickness increase.

TABLE I. Test of stressed III-V binary constituent media, with alike qualitative behavior under *keyboard* effect. The crystallographic growth planes and the in-plane direction of the heterostructure slab are indicated in the columns 4 and 5, respectively.

Figure	Substrate:Heterostructure	Growth	In-plane	Hole	VB-offset(eV)
Fig. 4	$InSb : InSb - AlN - InSb$	(111)	[11]	*lh*	$-253.6674\kappa_{\mathrm{T}}^2 + 1.1101$
Fig. 5	$InP : GaP - AlSb - GaP$	(001)	[10]	*lh*	$10.052\kappa_{\mathrm{T}}^2 - 0.057379$
Fig. 6	$InSb : GaP - AlAs - GaP$	(111)	[11]	*hh*	$8.804\kappa_{\mathrm{T}}^2 - 0.040337$
Fig. 7	$AlAs : InAs - AlN - InAs$	(111)	[10]	*lh*	$-135.6419\kappa_{\mathrm{T}}^2 + 3.3961$
Fig. 7	$InSb : InSb - AlAs - InSb$	(001)	[10]	*lh*	$-239.9757\kappa_{\mathrm{T}}^2 - 0.73231$
	$AlAs : InAs - AlAs - InAs$	(111)	[11]	*lh*	$-125.9776\kappa_{\mathrm{T}}^2 + 0.77702$
				hh	$-3.0689\kappa_{\mathrm{T}}^2 + 0.77702$
	$AlN : InAs - AlN - InAs$	(111)	[11]	*lh*	$-137.4486\kappa_{\mathrm{T}}^2 + 1.677$
				hh	$-6.219\kappa_{\mathrm{T}}^2 + 1.677$
	$AlP : InAs - AlP - InAs$	(111)	[11]	*lh*	$-128.9852\kappa_{\mathrm{T}}^2 + 0.91323$
				hh	$-3.3193\kappa_{\mathrm{T}}^2 + 0.91323$
	$AlSb : InAs - AlSb - InAs$	(111)	[11]	*lh*	$-116.2789\kappa_{\mathrm{T}}^2 + 0.44377$
				hh	$-1.484\kappa_{\mathrm{T}}^2 + 0.44377$
	$GaAs : InSb - AlAs - InSb$	(111)	[11]	*lh*	$-242.1964\kappa_{\mathrm{T}}^2 - 0.28447$
				hh	$-4.4541\kappa_{\mathrm{T}}^2 - 0.28447$
	$GaN : InSb - AlN - InSb$	(111)	[11]	*lh*	$-253.6674\kappa_{\mathrm{T}}^2 + 0.88565$
				hh	$-7.6042\kappa_{\mathrm{T}}^2 + 0.88565$
	$GaP : InSb - AlP - InSb$	(111)	[11]	*lh*	$-245.204\kappa_{\mathrm{T}}^2 - 0.13416$
				hh	$-4.7045\kappa_{\mathrm{T}}^2 - 0.13416$
	$InAs : InSb - AlSb - InSb$	(111)	[11]	*lh*	$-232.4977\kappa_{\mathrm{T}}^2 - 0.64776$
				hh	$-2.8692\kappa_{\mathrm{T}}^2 - 0.64776$
	$InP : GaP - AlP - GaP$	(111)	[11]	*lh*	$-14.116\kappa_{\mathrm{T}}^2 + 0.60962$
				hh	$8.5537\kappa_{\mathrm{T}}^2 + 0.60962$
	$AlAs : GaP - AlSb - GaP$	(001)	[10]	*lh*	$10.052\kappa_{\mathrm{T}}^2 - 0.0087943$
				hh	$-1.0727\kappa_{\mathrm{T}}^2 - 0.0087943$
	$GaAs : GaP - AlSb - GaP$	(001	[10]	*lh*	$10.052\kappa_{\mathrm{T}}^2 - 0.006966$
				hh	$-1.0727\kappa_{\mathrm{T}}^2 - 0.006966$
	$InP : GaP - AlSb - GaPb$	(001)	[10]	*lh*	$10.052\kappa_{\mathrm{T}}^2 - 0.057379$
				hh	$-1.0727\kappa_{\mathrm{T}}^2 - 0.057379$

Although not depicted here, we have found qualitative patterns alike *keyboard* effect under pseudomorphic strain, for several $III - V$ binary compounds (see Table I). As a bonus, a numerical evaluation of the polynomial interpolation (16) is presented in the last column of the Table I, thus complementing the characterization of the selected systems.

3.2. Influence of the pseudomorphic strain on k_z-spectrum

The QEP k_z-spectrum is a meaningful, and well-founded physical quantity that can be obtained *via* the *root-locus-like* procedure [19] by unfolding back in the complex plane the dispersion-curve values for bulk materials, determined by stress-induced effects on the stress-free heterostructure. Thus, we take advantage of the *root-locus-like* know-how, to promptly identify evanescent modes, keeping in mind that complex (or pure imaginary) solutions are forbidden for some layers and represent unstable solutions underlying the lack of hospitality of these slabs for oscillating modes. The opposite examination is straightforward and also suitable for propagating modes, which become equated with stable solutions for given layers.

To obtain the QEP k_z-spectrum in a periodic pseudomorphically strained heterostructures of QB-acting/QW-acting/QB-acting materials, we first use (10) and substitute it in $\widehat{\boldsymbol{W}}_{\mathrm{eff}}$ [13]. Next, we solve again the characteristic problem (9), whose eigenvalues allow us to obtain the new expression for the QEP-matrix $\boldsymbol{\mathcal{K}}$, and then finally consequently solve (2) for k_z. Once we have quoted the eigenvalues k_z of (7), it

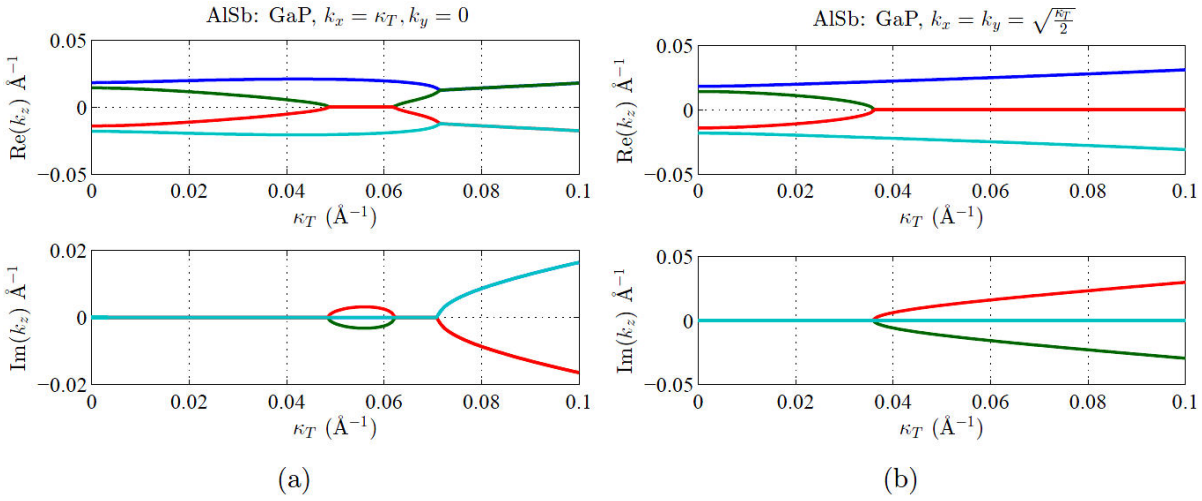

FIGURE 8. (Color online) Root locus for the eigenvalues k_z from QEP (7), as a function of κ_{T} for strained AlSb(substrate)/GaP (epitaxial layer). We had assumed $E = 0.6$ eV, and in-plane directions [10]/[01] for panel (a)/(b).

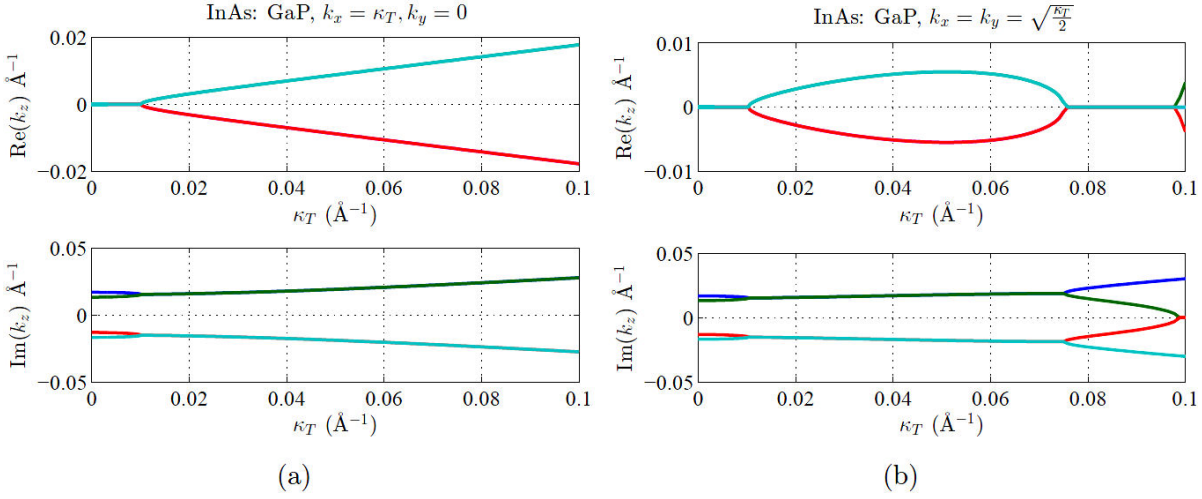

FIGURE 9. (Color online) Root locus for the eigenvalues k_z from QEP (7), as a function of κ_{T} for strained InAs(substrate)/GaP (epitaxial layer). We had assumed $E = 0.45$ eV, and in-plane directions [10]/[01] for panel (a)/(b).

is then straightforward to generate a plot in the complex plane, symbolizing the locations of k_z values that rise as band mixing parameter κ_{T} changes. Keeping in mind that complex (or pure imaginary)/real solutions of (7) represent forbidden/allowed modes, we take advantage of the *root-locus-like* map to identify evanescent/propagating modes for a given layer. Thus, we are able "to stamp" on a $2D$-map language, a frequency-domain analysis of the envisioned heterostructure under a quantum-transport problem. This way, we are presenting an unfamiliar methodology in the context of quantum solid state physics, to deal with low-dimensional physical phenomenology.

The Fig. 8 and 9 illustrate the role of band mixing for $\kappa_{\mathrm{T}} \left[10^{-6}, 10^{-1}\right]$ Å^{-1}, on the k_z spectrum from QEP (7) for a III-V strained alloy, clearly distinguished as QW in most layered systems of technological interest. Importantly, by assuming two different substrates AlSb (Fig. 8) and InAs (Fig. 9), we found different patterns of the k_z spectrum for lh and hh. Namely for the $[10]$ in-plane direction, the k_z *root-locus-like* evolution is real for lh, in the range of $\kappa_{\mathrm{T}} \in \left[10^{-6}, 0.049\right]$ Å^{-1} and $\kappa_{\mathrm{T}} \in [0623, 0.0708]$ Å^{-1}, while in the intervals $\kappa_{\mathrm{T}} \in [0.049, 0.0623]$ Å^{-1} and $\kappa_{\mathrm{T}} \in [0.0708, 0.1]$ Å^{-1}, k_z becomes pure imaginary and complex, respectively [see Fig. 8(a), inner green-red solid lines]. On the other hand, the k_z *root-locus-like* shows real values for hh, in the interval $\kappa_{\mathrm{T}} \in \left[10^{-6}, 0.0708\right]$ Å^{-1} and is complex, when $\kappa_{\mathrm{T}} \in [0.0708, 0.1]$ Å^{-1} [see Fig. 8(a) outer blue solid lines]. It is noteworthy that hh and lh curves are undistinguishable in this latter interval. Although not shown here, the $[01]$ in-plane direction exhibits the same behavior. The Fig. 8(b), displays the QEP (7 spectrum along the $[11]$ in-plane direction. For lh only, k_z *root-locus-like* evolution starts as a real number in the range $\kappa_{\mathrm{T}} \in \left[10^{-6}, 0.0363\right]$ Å^{-1}, and becomes pure imaginary for $\kappa_{\mathrm{T}} \in [0.0363, 0.1]$ Å^{-1}. The k_z spectrum for hh it is always a real number in the whole selected interval $\kappa_{\mathrm{T}} \in \left[10^{-6}, 0.1\right]$ Å^{-1}. Panel (a) of Fig. 9 describes

in-plane direction $[10]$ and by analogy the $[01]$ –although not depicted for brevity–, with the band mixing. For both lh and hh, the k_z evolution starts as a pure imaginary number in the range $\kappa_{\text{T}} \in \left[10^{-6}, 0.01\right]$ Å^{-1}, and becomes a complex number in the interval $\kappa_{\text{T}} \in [0.01, 0.1]$ Å^{-1}. In this gap the hh and lh are indistinguishable when their k_z magnitude is the same. Meanwhile, the panel (b) of Fig. 9 demonstrates that for the $[11]$ in-plane direction, the k_z values are mostly complex or pure imaginary, except in the small interval of $\kappa_{\text{T}} \in [0.097, 0.1]$ Å^{-1}, where they are real. No real entries of k_z for hh were found as κ_{T} changes within the bounds $[0.01, 0.1]$ Å^{-1}. The hh and lh curves are indistinguishable in the range of $\kappa_{\text{T}} \in [0.0133, 0.075]$ Å^{-1}. After this detailed description, several features deserve close attention. In short: the $[10]$ and $[01]$ in-plane directions show an isotropic behavior for each selected substrate. The real-value domains of the *root-locus-like* map of k_z means that the GaP strained-layer recovers its standard QW-behavior for both hh and lh quasiparticles in the stress-free configuration. On the opposite, whenever real-value map fades, *i.e.* complex or pure imaginary magnitudes arise, none oscillating modes can propagate through an InAs:GaP strained slabs. In this case, the GaP might turns into an effective QB for traveling holes.

For completeness, the pseudomorphic perturbation on several stress-free hexagonal heterostructures have been considered here and we found slight modifications in the band offset compared to the unstrained case for growth planes (0001) and (1m00). However, nor permutations of V_{eff} neither *keyboard* patterns were detected in such semiconductors materials.

3.3. Bandgap and valence-band offset manipulation

It has widely been accepted that electronic properties can be tuned by elastic stress. This assertion is clearly illustrated computationally for VB in Figs. 4, 5, 6 and 7, which exhibit modifications of the VB-offset whenever a biaxial-pseudomorphic strain is applied. Recently, some authors have addressed a first-principles density functional theory calculations to a monolayer of a MoS_2 and indicate that both direct and indirect bandgap decrease in the presence of biaxial strain, with transitions from direct to indirect bandgap [27]. As uniform stress leads to band-structure changes, we thereby expect the bandgap of exercised III-V heterostructures displayed in Figs. 4, 5, 6 and 7, to evolve from nominal unstrained crystal spectrum forbidden gap. It is worth noting that as shown independently in Fig. 3(c,d), the way to tune the V_{eff} profile as well as the VB offset is by letting grow the $hh - lh$ coupling. The latter represents a complementary tool, to that proposed before [27, 28] in manipulating the electronic structure, but this time for tensile strain-free systems. Importantly, VB-offset progression depicted in Figs. 3(c,d), 5(b) and 6 for III-nitride(antimonide) heterostructure, as one of its constituent media, demonstrates an anisotropic behavior, as a bonus to the expected differences between hh and lh, due to their effective masses.

In Subsecs. (3.1.2.) and (3.3.) we have shown the V_{eff} profile evolution and the *keyboard* effect under the competitors hole-mixing and strain. We hope that these appealing events would attract the attention of a wider community of physicists beyond condensed-matter theoreticians. The present graphic modelling of V_{eff} evolution, may be a reliable workbench for testing several configurations of materials with minor changes, if any, being useful in both experimental applications and in theoretical analysis. The latter means that rather than considering the present study as an end-in-itself theoretical exercise –which is not our goal–, readers working in complementary and even in different fields most use (16) for zinc blende, and (22) for wurtzite to quote V_{eff} eigenvalues from (9) and this way incorporate the mutable profile of V_{eff} instead of the commonly used fixed $\boldsymbol{V}(z) = V_{\text{B}} - V_{\text{A}}$. If the studies involve electronic properties and/or scattering processes, modifications of the conductance and thereby the tunneling time, should be expected by taking realistic V_{eff} mutable quantities derived from work out the eigenvalue problem (9)-(10) rather than take a constant-guess value $\boldsymbol{V}(z) = V_o$. We strongly recommend to include current results to further improve own researches that should be related to the real-world experiments and day-to-day applications.

4. Conclusions

We present an alternative graphic-based unambiguous theoretical procedure to demonstrate the VB-mixing and strain impact on V_{eff} metamorphosis. Have been accurately derived an analytic expression of the VB-offset for zinc blende semiconductors, while for the wurtzite its explicit *eigen*-values were deduced from the proper (6×6) Hamiltonian [24]. The *lh* experience the striking *keyboard* effect of V_{eff} in stress-free and stressed systems. Nevertheless, in strained heterostructures the former behavior have been also found for *hh*. Evidences of this sort foretell their usefulness in experimental applications such as: VB-profile tuning, VB-offset manipulation and in theoretical analysis of hole tunneling and spectrum. Pseudomorphic strain is able to diminish the *keyboard* effect and also makes it emerge or even vanish eventually. We remark that the multiband-mixing and stress-induced events, are strong concurrent appliances that can not be universally neglected in layered systems. Tuning in-plane directions the *keyboard* effect under strain reveals anisotropic and thereof topologically tunable. The present modelling of V_{eff} evolution, may be a reliable workbench for testing other configurations and may be of relevance for promising heterostructure's design guided by VB-structure modelling to enhance the hole mobility in III-V semiconducting devices provided they always lagged compared to II-IV media [8].

Acknowledgments

This work was developed under support of DINV, Universidad Iberoamericana (UIA), México. One of the authors (L.D-

C) is grateful to the Visiting Academic Program of the UIA, México.

1. G. Klicmeck, R. Ch. Bowen, and T.B. Boykin, *Superlattices and Microstructures* **29** (2001) 187.
2. R. Wessel and M. Altarelli, *Phys. Rev. B* **39** (1989) 12802.
3. H. Schneider, H.T. Grahn, K. Klitzing, and K. Ploog, *Phys. Rev. B* **40** (1982) 10040.
4. A.C. Bittencourt, A.M. Cohen and G.E. Marques, *Brazilian J. Phys.* **27** (1997) 281.
5. B.A. Foreman, *Phys. Rev. B* **76** (2007) 045327.
6. N.J. Ekins-Daukes *et al*., *App. Phys. Lett.* **75** (1999) 4195.
7. T.M. Smeeton, M.J. Kappers, J.S. Barnard, M.E. Vickers and C.J. Humphreys, *App. Phys. Lett.* **83** (2003) 5419.
8. Aneesh Nainani, Brian R. Bennett, J. Brad Boos, Mario G. Ancona and Krishna C. Saraswat, arxiv.org/pdf/1108.5507 (2011).
9. D.A. Faux, J.R. Downes and E.P. OReilly, *J. App. Phys.* **82** (1997) 3754.
10. Sunil Patil, W.P. Hong and S.H. Park, *Phys. Lett. A* **372** (2008) 4076.
11. Manish K. Bashna, Pratima Sen and P.K. Sen, *Indian J. Pure App. Phys.* **51** (2013) 553.
12. V. Milanović, and D. Tjapkin, *Phys. Stat. Sol(b)* **110** (1982) 687.
13. J.J. Flores-Godoy, A. Mendoza-Álvarez, L. Diago-Cisneros, and G. Fernández-Anaya *Phys. Status Solidi B*, **67** (2113) 1339.
14. R. Pérez-Álvarez and F. García-Moliner, *Transfer Matrix, Green Function and related techniques: Tools for the study of multilayer heterostructures*, (Ed. Universitat Jaume I, Castellón de la Plana, España, 2004).
15. S. Ekbote, M. Cahay and K. Roenker, *J. App. Phys.* **85** (1999) 924.
16. L. Diago-Cisneros, H. Rodríguez-Coppola, R. Pérez-Álvarez, and P. Pereyra, *Phys. Rev. B* **74** (2006) 045308.
17. K.H. Yoo, J.D. Albrecht and L.R. Ram-Mohan, *Am. J. Phys.* **78** (2010) 589.
18. V.D. Jovanović, *Quantum Wells, Wires and Dots*, (Ed. John Wiley & Sons, Ltd.), 2005.
19. A. Mendoza-Álvarez, J.J. Flores-Godoy, G. Fernández-Anaya, and L. Diago-Cisneros, *Phys. Scr.* **84** (2011) 055702.
20. L. Diago-Cisneros, H. Rodríguez-Coppola, R. Pérez-Álvarez and P. Pereyra, *Phys. Scr*. **71** (2005) 582.
21. O. Ambacher *et al*., *J. Phys.: Condens. Matter* **14** (2002) 3399.
22. Joachim Piprek, "*Semiconductor Optoelectronic Devices. Introduction to Physics and simulation*", (Ed. Elesevier, Acadenic Press), (2003).
23. I. Vurgaffman, J.R. Mayer, and L.R. Ram-Moham, *J. App. Phys.* **89** (2001) 5815.
24. Francisco Mireles and Sergio E. Ulloa, *Phys. Rev. B* **60** (1999) 13659.
25. D.A. Broido and L.J. Sham, *Phys. Rev. B* **31** (1985) 888.
26. Z. Ikonić, V. Milanović, and D. Tjapkin, *Phys. Rev. B* **46** (1992) 4285.
27. Ji Feng, Xiaofeng Qian, Cheng-Wei Huang and Ju Li, *Nature Photon.* **6** (2012) 866.
28. W.S. Yun, S.W. Han, S.C. Hong, I.G. Kim, and J.D. Lee, *Phys. Rev. B* **85** (2012) 033305.